Electronic Supplementary Material (ESI) for Nanoscale.

Collective excitation of plasmonic hot–spots for enhanced hot charge carrier transfer in metal/semiconductor contacts

Supporting Information

Adrien Piot,[†,‡] Suart Earl,[¶] Charlene Ng,[§,‡] Svetlana Dligatch,[‖] Ann Roberts,[¶] Timothy J. Davis,[§,‡] and Daniel E. Gómez[*,§,‡]

Institut National des Sciences Appliquées de Toulouse, 135 Avenue de Rangueil, 31400, Tolouse, France, Melbourne Centre for Nanofabrication, Australian National Fabrication Facility, Clayton VIC 3168, Australia, School of Physics, The University of Melbourne, Parkville, VIC, 3010, Australia, CSIRO, Manufacturing Flagship, Private Bag 33, Clayton, VIC, 3168, Australia, and CSIRO, Manufacturing Flagship, PO Box 218, Lindfield NSW 2070, Australia

E-mail: daniel.gomez@csiro.au

[*]To whom correspondence should be addressed
[†]Institut National des Sciences Appliquées de Toulouse, 135 Avenue de Rangueil, 31400, Tolouse, France
[‡]Melbourne Centre for Nanofabrication, Australian National Fabrication Facility, Clayton VIC 3168, Australia
[¶]School of Physics, The University of Melbourne, Parkville, VIC, 3010, Australia
[§]CSIRO, Manufacturing Flagship, Private Bag 33, Clayton, VIC, 3168, Australia
[‖]CSIRO, Manufacturing Flagship, PO Box 218, Lindfield NSW 2070, Australia

Hot–electron injection probability To estimate the efficiency of hot–electron injection from the Al nanodimers into the underlying TiO_2 film, we apply the model of White and Catchpole (WC)[1] where several simplifiying assumptions are made. The parameters required for the estimation are the Al work function -4.28 eV (also for reference we use the one for Au -5.1 eV)[2] and the position of the conduction band of TiO_2 -4.14 eV[3]

(A)

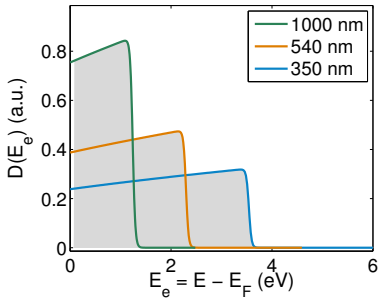

(B)

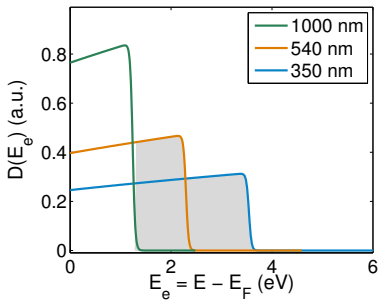

(C)

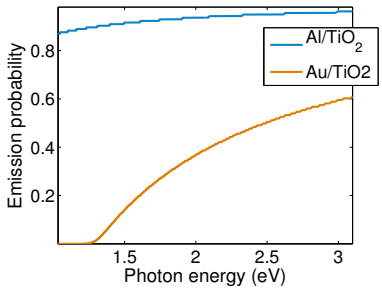

Figure S1: (A) Density of energy (E_e) states D of the hot–electron in Al nanoparticles shown for three incident photon wavelengths (350 nm, 540 nm and 1000 nm). The energy scale is relative to the Fermi level E_F of the metal. The shaded areas correspond to those electrons with energies above the Al/TiO_2 Schottky barrier. (B) Similar to (A) but plotted for the case of Au. (C) Hot–electron emission probability [$\eta(\lambda)$ in eqn. (S1)] as a function of incident photon energy.

According to WC,[1] the metal–to–semiconductor hot–electron photo–current density j_{sc}

can be estimated according to:

$$j_{sc} = e \int S(\lambda)\sigma_{abs}(\lambda)\eta(\lambda)d\lambda, \tag{S1}$$

where e is the electron's charge, $S(\lambda)$ is the incident photon flux on the plasmonic system (number of photons / (s nm μm^2)). In our study this is determined by the intensity of the Hg lamp and the bandpass filter between the lamp and the plasmonic system. $\sigma_{abs}(\lambda)$ is the absorption cross-section (μm^2) of the plasmonic array and $\eta(\lambda)$ is the probability of hot–electron emission from the metal nanoparticles into the TiO_2 substrate. η is defined as the fraction of photo–excited electrons with sufficient energies above the metal Fermi level to overcome the Schottky energy barrier ϕ_{SB} of fig. 1. This fraction is shown in the shaded areas of the top two graphs of fig S1. The hot–electron transfer probability is shown in fig. S1(C) for the cases of Al/TiO_2 and Au/TiO_2. Due to the greatly reduced Schottky barrier height, the hot–electron emission probability is much higher for Al than for Au across the entire spectrum.

Rigorous Coupled Wave Analysis The optical properties of the plasmonic structures were simulated using the Matlab routines provided in RETICOLO:[4–6] an implementation of a frequency–domain Rigorous Coupled Wave Analysis. This method, relies on a scattering matrix approach to related mode amplitudes across layers in the structures. The modes in each layer are in turn computed using Fourier expansions (plane waves).

TiO_2 thin film deposition TiO_2 films were deposited at $\sim$ 1.5 Å/sec rate at a temperature of 200 °C in an electron beam evaporation system of in–house construction. An oxygen partial pressure was automatically maintained at $\sim$ 5x10^{-5} Torr throughout the deposition. The substrate temperature was measured indirectly using a thermocouple and both the thickness and deposition rate were measured with a quartz crystal monitor. During the deposition, the film thickness was indirectly measured by in–situ transmittance monitoring. Finally, the films were annealed at 450 °C after deposition.

To characterise the structure of the films, XRD was performed resulting in the data shown in fig. S2. The XRD scan for the un–annealed sample shows presence of Anatase. On the contrary, the XRD scan of the film annealed at 450 °C indicated that some re-crystallisation is taking place (as expected) and Rutile phase starts to appear. The Rutile R(1 1 0) peak is not present in the as–deposited film XRD measurements. The XRD spectrum of the annealed sample shows the presence of a small R(1 1 0) peak at 27.4 degrees.

(A)

(B)

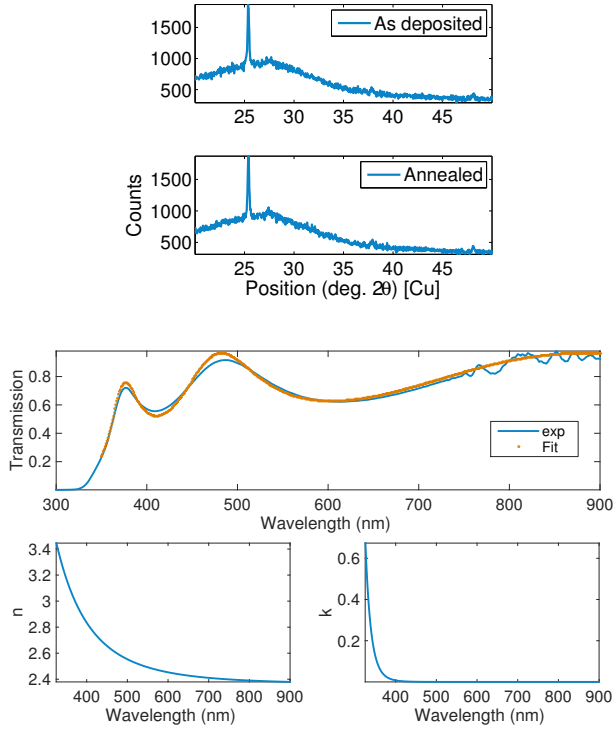

Figure S2: (A) XRD scans of the TiO_2films before (top) and after (bottom) thermal annealing. Annealing results in re–crystallization and the formation of Rutile phases. (B) Normal incidence transmission spectra of the resulting thin films along with a calculated transmission spectrum. The lower two panels are the complex refractive index calculated for TiO_2 using a Cauchy model for this thin film.

Nanofabrication details 3 mm x 3 mm periodic arrays of nanorod dimers were fabricated by electron beam lithography using a Vistec EBPG 5000 plus ES (100 keV, 3 nA) using a double–layer positive resist consisting of 50 nm of poly(methyl methacrylate) (Micro-Chem, 950k A2) on top of 110 nm of methyl methacrylate (Micro-Chem, MMA(8.5) MAA EL6), spin coated on top of the TiO_2 films. The exposed patterns were developed with

a 1:3 methyl isobutyl ketone/ isopropanol solution for 60 s, rinsed by ultrasonication with isopropanol, and dried with a nitrogen gun. 40 nm of Al were deposited by electron beam evaporation (no adhesion layer was used). The final step in the nanofabrication consisted on a lift off step with acetone/anisole. The structures were characterised by scanning electron microscopy (FEI, Nova NanoSEM 430).

Transmission measurements Measurements of normal incidence transmission spectra T were carried out using a spectroscopic ellipsometer (J. A. Woolam Co. M2000-DI). For the normal incidence spectra, the samples were mounted on a transmission stage and the reference background measurement was done in an area adjacent to the plasmonic array, i.e. on the bare TiO_2 film which has a transmission spectrum shown in fig. S2(B).

Decomposition of methylene blue

A Polydimethylsiloxane (PDMS) micro–fluidic chip was bonded on top of the slide supporting the array of Al nanoparticles. A volume of ~ 100 μL of 50 ppm of methylene blue (MB) in water was deposited through the microfluidic channel in order to completely fill the area covered by the plasmonic array. This system was left undisturbed in the dark to allow for adsorption/desorption equilibration. Light from a 100 W Hg lamp was spectrally filtered with a band pass filter (Thorlabs FB550-40) and was used for illuminating the sample as indicated in fig. S3. The intensity of this illumination was 3.42 mW/cm^2. An attenuated Xe lamp (20 W) was employed for measuring the transmission spectrum (T) across the sample as a function of time (t) using a monochromator (Acton SP2300) equipped with a CCD detector (Pixis 1024)

The measured change in absorbance ΔA shown in fig 3 is given by Beer-Lambert's law:

$$\Delta A(t) = A(t) - A(t=0) = \epsilon b \left(C(t) - C(0)\right) = -\log_{10}\left[\frac{T(0)}{T(t)}\right], \tag{S2}$$

where ϵ is the molar extinction coefficient of MB, b is the optical path length in the measurement of the transmission T spectra and $C(t)$ is the concentration. MB has a known molar

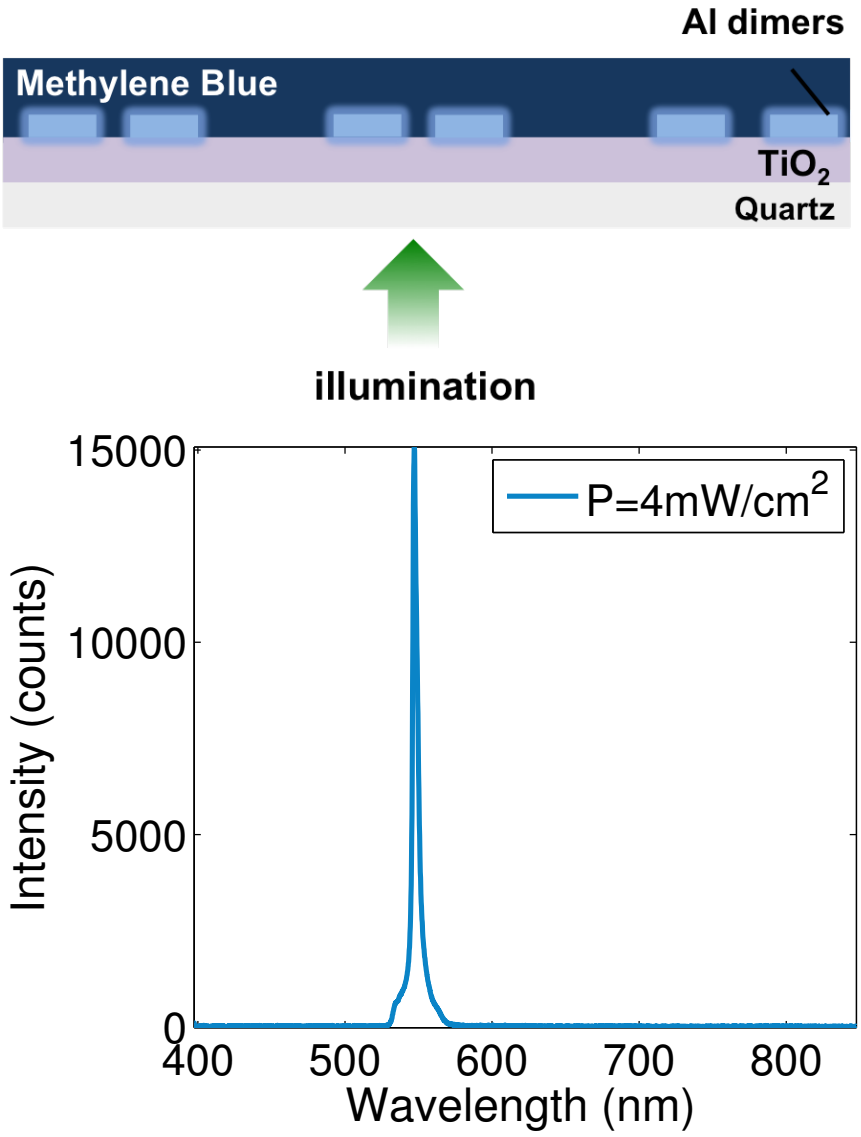

Figure S3: Schematic representation of the experimental configuration for the measurement of the decomposition of MB.

extinction coefficient at 660 nm of 10^5 $dm^3(mol\ cm)$[17]

When the kinetics of the reaction is of first–order, the above equation can be written as:

$$\Delta A(t) = \epsilon b C(t=0)\left(e^{-kt} - 1\right), \tag{S3}$$

which faithfully reproduces the measured decay for the bare TiO_2 substrate, yielding a rate constant of $k = 5.6 \times 10^{-6} s^{-1}$.

On the contrary, for the region containing the Al dimer array, we found that the change in absorbance (and thus concentration) was better described by a bi–exponential decay:

$$\Delta A(t) = \epsilon b C(t=0)(a\exp(-k_1 t) + (1-a)\exp(-k_2 t) - 1), \tag{S4}$$

which yields the following values $a = 7 \times 10^{-3}$, $k_1 = 1.13 \times 10^{-1} s^{-1}$ and $k_2 = 1.28 \times 10^{-5} s^{-1}$. From this bi–exponential fit, one can define an average decay rate as:$\langle k \rangle = ak_1 + (1-a)k_2$ which yields $\langle k \rangle = 8.18 \times 10^{-4} s^{-1}$ a value that is ~ 150 times larger than the one found for the bare TiO_2 substrate.

References

(1) White, T. P.; Catchpole, K. R. *Applied Physics Letters* **2012**, *101*, 073905.

(2) Michaelson, H. B. *Journal of Applied Physics* **1977**, *48*, 4729–4733.

(3) Zhang, X.; Chen, Y. L.; Liu, R.-S.; Tsai, D. P. *Reports on Progress in Physics* **2013**, *76*, 046401.

(4) Lalanne, P.; Jurek, M. P. *Journal of Modern Optics* **1998**, *45*, 1357–1374.

(5) Lalanne, P.; Morris, G. M. *J. Opt. Soc. Am. A* **1996**, *13*, 779–784.

(6) Moharam, M. G.; Gaylord, T. K.; Grann, E. B.; Pommet, D. A. *J. Opt. Soc. Am. A* **1995**, *12*, 1068–1076.

(7) Mills, A.; Wang, J. *Journal of Photochemistry and Photobiology A: Chemistry* **1999**, *127*, 123 – 134.